Nanoscale

COMMUNICATION

View Article Online
View Journal | View Issue

Cite this: *Nanoscale*, 2016, **8**, 15850

Received 15th May 2016,
Accepted 30th July 2016

DOI: 10.1039/c6nr03935a

www.rsc.org/nanoscale

Highly stretchable, printable nanowire array optical polarizers†

Soonshin Kwon,*[a] Dylan Lu,[b] Zhelin Sun,[b] Jie Xiang[b] and Zhaowei Liu*[b]

Designing optical components such as polarizers on substrates with high mechanical deformability have potential to realize new device platforms in photonics, wearable electronics, and sensors. Conventional manufacturing approaches that rely highly on top-down lithography, deposition and the etching process can easily confront compatibility issues and high fabrication complexity. Therefore, an alternative integration scheme is necessary. Here, we demonstrate fabrication of highly flexible and stretchable wire grid polarizers (WGPs) by printing bottom-up grown Ge or Ge/Si core/shell nanowires (NWs) on device substrates in a highly dense and aligned fashion. The maximum contrast ratio of 104 between transverse electric (TE) and transverse magnetic (TM) fields and above 99% (maximum 99.7%) of light blocking efficiency across the visible spectrum range are achieved. Further systematic analyses are performed both in experimental and numerical models to reveal the correspondence between physical factors (coverage ratio of NW arrays and diameter) and polarization efficiency. Moreover, we demonstrate distinctive merits of our approach: (i) high flexibility in the choice of substrates such as glass, plastic, or elastomer; (ii) easy combination with additional novel functionalities, for example, air permeability, flexibility/stretchability, biocompatibility, and a skin-like low mechanical modulus; (iii) selective printing of polarizers on a designated local area.

Polarizers are one of the most commonly used elements that enable control of light in various optical instruments and display systems. The wire grid polarizer (WGP), since invented in mid-1920s by Land,[1] has become a major component in modern liquid crystal displays (LCDs) to modulate visual feedback in the realm of ubiquitous personal and mobile computing.[2,3] Recently, innovations in consumer portable and wearable electronic products have demanded the development of electronic and photonic components that are compatible with a variety of new solid-state substrates, for example in the form of glasses, clothing, and adhesive patches. Such a circumstance introduces new process requirements in device fabrication such as biocompatibility, versatility in substrate choices, flexibility/stretchability, mechanical softness and air permeability.[4,5] The traditional top-down semiconductor manufacturing approaches, however, encounter difficulties in harmonizing with these new guidelines due to the monolithic nature of the individual processing steps that render material choices limited by thermal budget constraints or material lattice mismatch constraints, and geometry choices limited to planar substrates.[6] Therefore, new design and fabrication strategies to achieve these compatibility requirements are essential to fulfill the trends of upcoming new device platforms. The design of device components through nanostructure assembly *via* a bottom-up approach such as from well-ordered nanowires or nanocolloids can provide alternative routes to overcome the drawbacks of traditional fabrication systems and introduce novel functionalities such as ballistic transport,[7] nanoscale energy conversion,[8] nanoelectromechanical systems,[9] phonon engineering,[10] tunable light emission and absorption,[11] and high detection sensitivity.[12] In order to gain better process efficiency and higher precision in controlling these bottom-up building blocks integrated into macroscale functional systems in the fields of nanoelectronics and photonics, intense efforts have been focused on the development of various methods, for example, Langmuir–Blodgett,[13] micro fluidic,[14] ink-jet,[15] dielectrophoresis,[16] self-assembly,[17] and contact printing.[18]

Semiconductor NWs, by virtue of their high aspect ratio and a thickness less than a few tens of nanometers, have demonstrated themselves as an excellent flexible device component.[19–21] Moreover, intensive studies on optical properties of these nanowires reveal their unique characteristics as a light absorber and scattering source correlated to their shape and geometry.[22,23] Barrelet *et al.* have shown the low loss waveguide nature of CdS NWs from direct measurement of the light guiding effect along the length direction of NWs.[23] Cao *et al.* demonstrated the resonance behavior of Ge and

[a]*Department of Mechanical and Aerospace Engineering, University of California, San Diego, La Jolla, California 92093, USA. E-mail: sok026@ucsd.edu*
[b]*Department of Electrical and Computer Engineering, University of California, San Diego, La Jolla, California 92093, USA. E-mail: zhaowei@ucsd.edu*
†Electronic supplementary information (ESI) available. See DOI: 10.1039/c6nr03935a

Si NWs showing strong polarization sensitive absorption and scattering spectra in the visible range.[24] Both the high mechanical flexibility and optical cavity resonator effect prove semiconductor NWs as excellent building blocks for wearable/printable optoelectronics. In addition, a wide range of choices for geometrical dimension, material composition, and heterostructure provide highly tunable optical behaviors such as transmission/absorption spectrum and resonance modes.[25–27] Several fundamental studies were made on the polarization effect of semiconductor NWs,[28–30] however, there was no direct integration of polarization properties of NWs into a macroscopic device system.

Here, we demonstrate a new design concept of WGPs using Ge or Ge/Si core/shell NWs combined with a simple and robust printing method creating arrays of aligned NWs in a subwavelength pitch size. Integration of these finely printed NW arrays on transparent substrates, such as polyethylene terephthalate (PET) and poly(dimethylsiloxane) (PDMS) elastomer, enables the design of mechanically soft optical filters with multi-functional and human-friendly characteristics such as biocompatibility,[31] air permeability,[4] stretchability, and conformal lamination on a curvy substrate. Assembled NW arrays show a misalignment of 3°–7° to implement a high quality optical polarizer with a contrast difference exceeding 100 times between transverse electric (TE) and transverse magnetic (TM) modes and blocking efficiency of 99.7% against incident TE light across the visible spectrum range. We have further systematically studied the performance of our NW WGPs related to internal device parameters (NW coverage/diameter) and investigated the optical characteristics of NW polarizers under high mechanical deformation such as folded, curved, and stretched circumstances. Our new design concept and fabrication approach can provide a novel route for the development of wearable electronics at the human–device interface and in communication systems.

Inspired by the aforementioned advantages of semiconductor NWs, we have successfully fabricated NW-PET/NW-PDMS WGPs as shown in Fig. 1. The overall fabrication process is depicted in Fig. 1a. Either Ge or Ge/Si core/shell NWs were synthesized by a chemical vapour deposition process using a vapour–liquid–solid method. Ge NWs were grown on Si substrates using 2% of GeH_4 in hydrogen as a precursor gas source at 290 °C and 300 Torr for 2 hours. Ge/Si core/shell NWs were synthesized by growing ~2 nm of the Si shell on the Ge core at 465 °C and 100 Torr using diluted SiH_4 (2% in hydrogen) for 10 min. The size of Ge NWs was

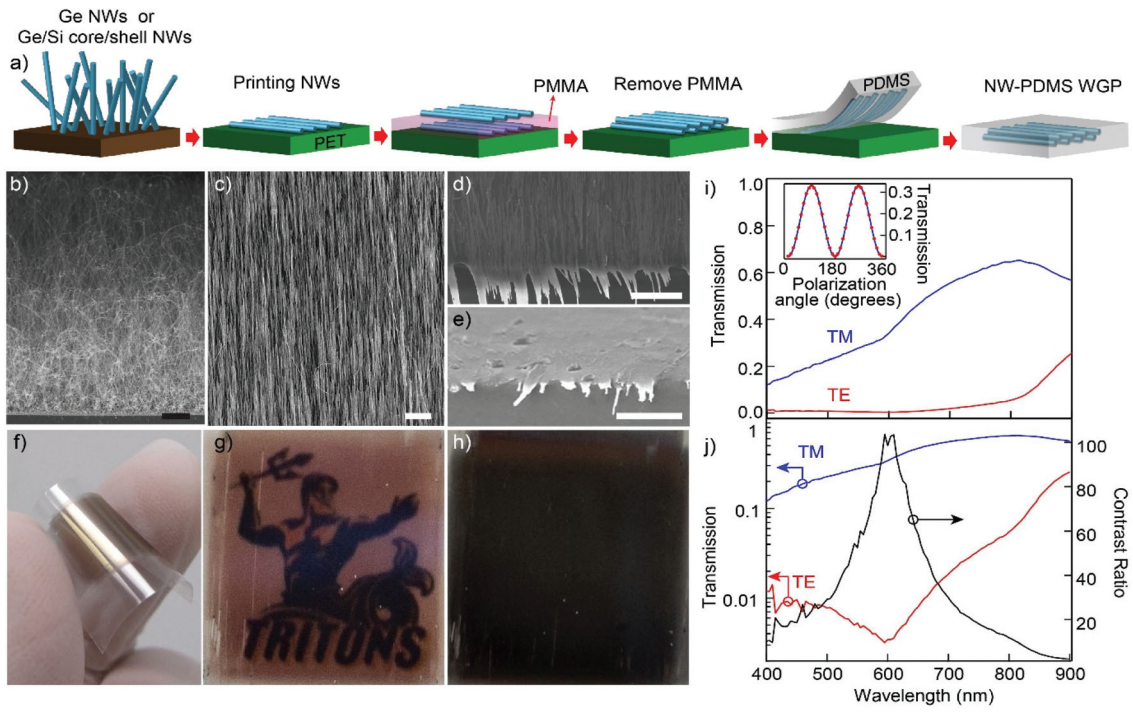

Fig. 1 NW WGP fabrication and optical transmission characterization. (a) Schematics of the fabrication process of a printed NW WGP on a plastic (PET) or elastomer (PDMS). Multiple printing of randomly oriented NWs on the grown substrates mediated by PMMA sacrificial layers that are transferred on a PET sheet and finally embedded in PDMS. SEM images of (b) as grown Ge NWs before transfer (90° tilted-view), a NW WGP on (c) PET and (d) PDMS showing a compact and highly ordered NW array. (e) SEM image under the 45° tilted-view shows an embedded NW array beneath the PDMS surface. All scale bars are 10 μm. (f) Photography of the NW WGP on a thin PET sheet. (g, h) Demonstration of the printed NW WGP for TM and TE-polarized incident wave assisted by one commercial polarizer positioned on top of the NW WGP. (i) Linear scale of TM (blue line) and TE (red line) transmission spectra of a NW polarizer. Inset shows measured polarization angle dependent transmission at a wavelength of 595 nm (red dashed line) in agreement with a calculated curve from Malus' law ($I = I_0 \cos 2\theta$; blue solid line). (j) log scale of TM (blue line) and TE (red line) transmission spectra of the NW polarizer, and their contrast ratio (black line).

controlled by using gold colloids (Ted Pella) ranging from 15–40 nm in diameter. 60–80 μm long NWs (Fig. 1b) were grown on a 4 inch wafer and the wafer was further diced into 2–5 cm square pieces for printing on a transparent ~150 μm thick PET substrate. To transfer the randomly oriented NW forest onto the PET substrate in a compact and parallel manner, we use mechanical contact transfer[32] where donor substrates (Si substrates with as-grown NWs) are slid over the receiver substrate (PET) by a directional shear force. The van der Waals force between NWs and the receiver substrate plays a major role in the NW alignment by first anchoring the free-standing end portion of NWs on the surface of the receiver substrate followed by landing the remaining portion of the NW body across the printing zone of a directional sliding with a speed of 1–2 mm s^{-1}.

For high polarizer performance, it is crucial to achieve a pitch distance less than the wavelength of incoming light with a minimized optical loss and a high contrast ratio (ratio of TM over TE transmission) by increasing NW array density. We have adopted a multiple printing scheme combined with intermediate sacrificial layers to dramatically improve the NW alignment density. This method provides significant improvement in the transmission contrast ratio of TE mode to TM mode by 10 times compared to without sacrificial layers. The purpose of introducing intermediate layers in the process of NW printing is to provide a fresh surface for maintaining high transfer yield and preventing friction among NWs[32] which otherwise hinders the increase of NW array density. Polymethyl methacrylate (PMMA) used as intermediate layers was spin-coated 5–7 times between the multiple NW printing and after the whole printing process is completed, PMMA layers were removed by gentle oxygen plasma treatment (20 W, 5–10 min). The top view SEM image of Fig. 1c shows a highly aligned and compacted NW array achieved by a sacrificial layer assisted multiple-printing process.

Fabrication of NW-PDMS WGPs can be realized subsequently from the NW-PET WGPs. Printing NWs directly on the PDMS results in a disordered NW film because of the highly adhesive surface of PDMS. This issue can be effectively solved by applying liquid PDMS to the NW-PET substrate and lifting off the cured NW-PDMS film from the PET. To realize this, first, a viscous PDMS–curing agent mixture (mixed in 10 : 1 ratio) was poured on top of the NW-PET WGPs followed by spinning to control the NW-PDMS film thickness. After spinning, NW-PDMS was left under vacuum without heat treatment for ~3 hours to achieve full infiltration of liquid PDMS between NWs. Finally, NW-PDMS was cured at 50 °C for 30 min and gently peeled off from the PET substrate. The result of the NW incubated PDMS film is displayed in Fig. 1d showing a well-aligned and highly compacted NW array. The smooth surface under the 45° tilted view in Fig. 1e shows complete embedding of the NW array into PDMS, which indicates that the liquid phase PDMS was fully infiltrated into the NW array to form a robust NW-PDMS film. Fig. 1f shows one sample image of a highly dense and well-ordered Ge NW array on a PET substrate visualizing a reddish brown colour. The demonstration of a fully functional NW WGP is displayed in Fig. 1g and h under TM and TE polarized light respectively. The clear visibility difference of the background image between TE and TM illuminations demonstrates the high blocking efficiency of a NW optical filter across the visible wavelength range and further illuminates the potential of this fabrication technique for high performance WGPs. Quantitative characterization of the NW WGP is shown in Fig. 1i and j (see the ESI† for the measurement set up). Fig. 1i displays measured transmission spectra under TM and TE incidence across the visible wavelength. The coefficient for TM transmission gradually increases from 12% to 55% across the visible range (from 400 nm to 700 nm) while TE transmission shows a minimum near 600 nm wavelength. The blocking of TE-polarized light is more obvious in a log scale where the light transmission is below 1% across 400 nm to 650 nm with a minimum of 0.3% at 595 nm wavelength. The contrast ratio between TM and TE light is also displayed in Fig. 1j showing a maximum of 104 at 595 nm. This implies that the bandwidth characteristic of a NW polarizer is dominated by the blocking of the TE-polarization which is determined by the dielectric dispersion response of the Ge NW array. The inset of Fig. 1j shows the measured polarization angle dependence of transmission (red dotted line) in agreement with a calculated curve from Malus' law[33] (blue solid line).

The polarizing mechanism of these dielectric NWs is similar to metallic grids in terms of utilizing anisotropic light interaction such that only a TM component vertically aligned to the grid can pass through the filter. However, in a microscopic view, while metallic grids mainly achieve their polarization effect by oscillating free electrons in response to the incoming light within the skin depth (2–3 nm),[34,35] polarization of Ge NWs is from absorption/scattering through the multiple internal reflections of photons along the length of NWs[36,37] originated from a high contrast of the dielectric constant between NWs and their surroundings. To gain quantitative understanding of the semiconductor NW WGPs and their polarizer performance, we first analyse the effect of NW spatial coverage on the polarization efficiency defined as ν = (TM − TE)/(TM + TE). In Fig. 2a, 7 samples with varying fill factors (ratio of covered area by NW arrays to the whole region of investigation under SEM) are chosen to explore how the spatial distribution of NW arrays affects the polarization efficiency. Estimation of the fill factor from each SEM image was performed by using the threshold tool in imageJ image processing software.[38] The degree of misalignments for all samples is controlled to be less than 7° analysed by the fast Fourier transform technique.[39] For the accuracy of the study, the incident beam spot was marked on each measured sample prior to the measurements and corresponding identification of the NW density and degree of alignment by SEM. As the portion of the covered area increases from 6% to 78%, the polarization efficiency rises linearly from 0.08 to 0.84. Side by side SEM images corresponding to each data point also visualize the difference in NW coverage while maintaining a similar degree of alignment.

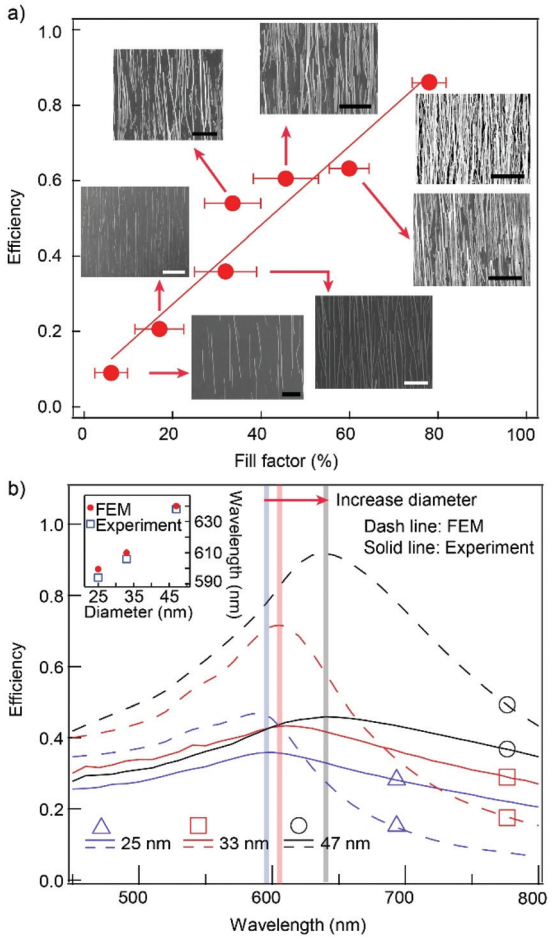

Fig. 2 Effect of geometric factors (NW filling density and size distribution) of Ge NW arrays on the polarization efficiency. (a) The NW fill factor *versus* efficiency where SEM images are presented next to each corresponding data point. Error bars represent the averaged fill factor from a series of SEM images taken within the beam spot area. All scale bars, 2 μm. (b) Polarizer efficiency as a function of NW diameter. Three samples with average NW sizes of 47 nm (black, circle), 33 nm (red, square), and 25 nm (blue, triangle) are studied both experimentally and numerically. Measurement and FEM simulation results are displayed in solid and dashed lines, respectively. Left top inset shows the shift of the wavelength position at maxima of efficiency curves.

In a single Ge NW photocavity, there is a tendency of red shift in the absorption spectrum correlated to the increase in the diameter of a single NW caused by a photon confinement effect.[24] Our interest, therefore, is to explore the polarization characteristics of these quasi-periodic and mono-layer dispersed arrays of Ge NWs linked to their size dispersion of Ge dielectrics. In Fig. 2b, three NW WGPs with distinctive NW diameter distributions of 25 ± 7 nm, 33 ± 8 nm, and 47 ± 9 nm were chosen to compare the spectrum of measured polarization efficiency accompanied with two-dimensional finite element modelling (FEM). NW arrays of three diameters, 25 nm, 33 nm, and 47 nm are controlled to have misalignments of 3.5°, 4.8°, and 5.8° and periods of 259 ± 132 nm, 248 ± 115 nm, and 255 ± 93 nm respectively in order to highlight the size effect of NWs on the polarization spectrum. The FEM model assumes infinitely long Ge NWs in parallel with the NW diameter and pitch to pitch distance provided by the SEM study. The dispersive permittivity of bulk Ge with both the real and imaginary parts[40] is used and the zeroth-order transmission is calculated. In Fig. 2b, the experimental results show broader and lower efficiency spectra compared to the simulated results. This is mainly due to the relatively large standard deviation in NW diameters and their array periods in the real samples which causes an averaging effect and additional light leakage path not presented in the simulation. From both experimental and numerical calculations, the efficiency spectra show a linear red shift behaviour from 600 nm to 640 nm as the NW diameter increases. Such a size effect is due to the increase in the dielectric response of the NW array to the incoming light for a larger diameter which causes a greater spectrum shift (see the ESI: Fig. S2a and S2b†). The study on the size effect of NW arrays provides an insight into optimizing the design of NW arrays as optical filters. For example, a broadband polarizer can benefit from increasing size distribution to achieve the broadened transmission profile, whereas colour filters that require a narrow bandwidth can gain merit by narrowing size distribution. The results also specifically demonstrate that a smaller size is preferable for a Ge NW array in the case of visible polarizer application because the polarization effect appears more dominant in a shorter wavelength range.

One of the distinctive merits of NW-PDMS WGPs apart from the traditional design on the rigid substrates is a high degree of deformability that originates from the low mechanical modulus of PDMS and softness of NWs.[41,42] The overall thickness of NW-PDMS films can be shrunk down to a few mm or even hundreds of μm thin to make a conformal contact on a curvy surface. In order to demonstrate this characteristic, we overlay the NW-PDMS WGP on spherical glassware with 1.25 cm of radius of curvature or a folded transparent plastic sheet as shown in Fig. 3a and b. The polarization effect is visualized by overlapping and rotating an additional commercial polarizer under room-light. Noticeably, Fig. 3a and b show that both WGPs are well adhered without any lift off from the high curvature surface caused by stretching/bending stress. Within such configurations, the polarization performance is still highly retained as the background image since the TM mode (center) is clearly visible compared with near zero visibility for the TE mode (right). For practical demonstration, two NW-PDMS WGPs 90° off phase to each other are attached onto two curved glass lenses of 1 inch in diameter and aligned side by side to mimic a smart contact lens for the three-dimensional virtual imaging effect as shown in Fig. 3c–e. In general, 3D display is achieved by creating an illusion of depth with a slightly different image to each eye while in our case two different images are used to verify the operation of two WGPs respectively. Fig. 3d and e clearly demonstrate the high performance of the NW-PDMS WGP visualizing/blocking two different side-by-side background images while the reddish brown colour is originated from the dielectric dispersive

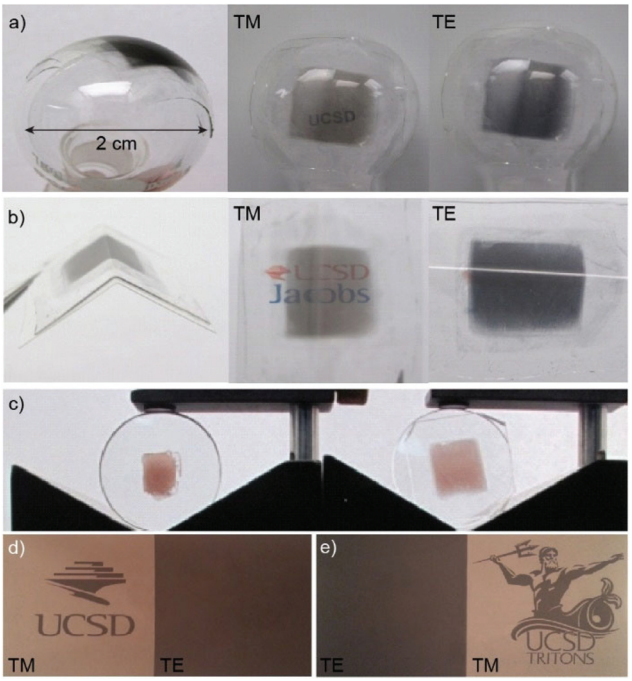

Fig. 3 Performance and applications of NW-PDMS WGPs. (a) NW-PDMS WGPs laminated on spherical glassware with 1.25 cm of radius of curvature and (b) on a fold plastic sheet. Polarizer performance under TM (center column) and TE (right column) transmission are shown. (c–e) Demonstration of NW-PDMS WGPs in a three-dimensional imaging system. Two NW-PDMS WGPs 90° off phase to each other are adhered on the surface of curved lenses and positioned side by side. An additional polarizer covers two images and is rotated 90° to modulate TM and TE polarized conditions.

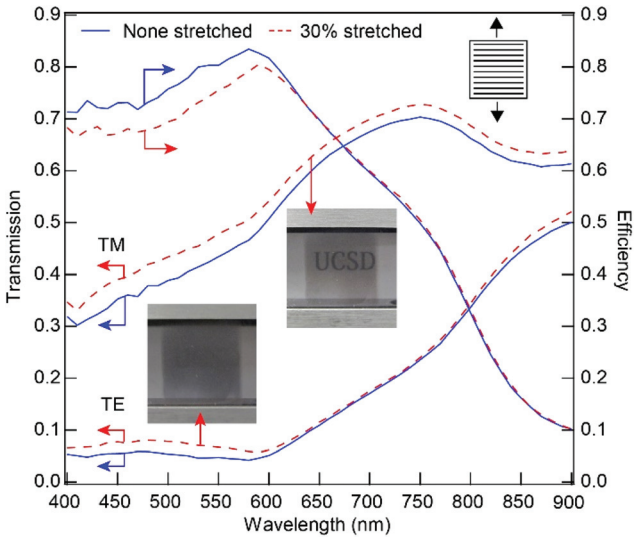

Fig. 4 NW-PDMS WGP transmission and efficiency spectra before and after stretching. Strain orientation is vertical to the NW alignment direction indicated in the top right inset. Solid and dashed lines represent performances at non-stretched (solid lines) and 30% stretched (dotted lines) cases, respectively. Two photographs visualize the performances of the NW-PDMS polarizer at the 30% stretched condition under TM (right) and TE (left) polarization. For demonstration, an additional commercial polarizer is positioned on top of the NW-PDMS WGP and rotated 90°.

properties of Ge NWs. To explore such excellent mechanical adaptability of the NW WGP in a more quantitative manner, we examine the TM/TE transmission and polarization efficiency of NW-PDMS WGPs as a function of strain displayed in Fig. 4. The stretching direction was chosen vertical to the length of the NW array as shown in the top right inset of Fig. 4 which is expected to have a more dramatic effect on polarization performance than pulling in parallel to the NW lateral axis. To acquire reliable measurements, the two ends of the NW-PDMS film are fastened on the stretching instrument and pre-examined to check that there is no detachment after stretching and releasing of the film. Transmission spectra are measured at each step of stretching among a total of 6 steps from 0 to 30% strain as shown in ESI Fig. S2† and finally measured when the film is released back to zero strain. During the stretching from 0 to 30% at 600 nm wavelength, the transmission for TM and TE show a gradual linear increase from 50.7% to 54.1% and 5.1% to 6.2% respectively. After strain is released back to zero, transmission intensities of TM and TE match the original values implying that the stretching is done in the elastic regime of the polarizer film demonstrating both high mechanical flexibility and durability. Comparison between non-stretched and 30% stretched cases over the visible spectrum range for TM, TE, and polarization efficiency is presented in Fig. 4. The study reveals that a slight decrease in efficiency starts to appear below 620 nm wavelength and from 400 to

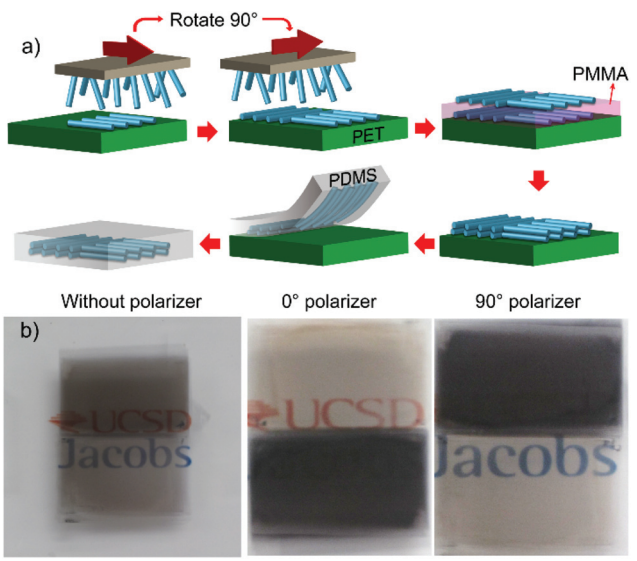

Fig. 5 Dual phase printing of NW-PDMS WGPs. (a) Schematics of the fabrication process. Arrays of NWs are printed on two designated neighbouring areas on a PET sheet followed by a final transfer to PDMS and peeling off. (b) Demonstration of the dual phase NW polarizer designed on a PDMS sheet. From left to right photographs show the WGPs under unpolarized, 0°, and 90° phase polarized light.

560 nm the percentage of efficiency loss is around 7.0 ± 1.2 after 30% strain while above 630 nm there is negligible loss. Since the period of NW grids should be less than $\lambda/2$ to work as a polarizer,[4] the measurement indicates that the average period of the NW array still maintains a subwavelength feature even at 30% of elastic tensile strain.

In addition to the soft conformal contact and stretchability, NW-PDMS WGPs are eligible for printing selectively on a targeted local area with a preferable polarizing orientation similar to simple imprinting of a mold on a substrate. This new concept provides micro-patterning of polarizers creating a localized screening/visualization effect of information displays with an advantage of a simple fabrication process. This concept is shown in Fig. 5a. For the demonstration, two sequential printings of NW-WGPs were performed side-by-side on a PET sheet with 90° off alignment followed by PDMS incubation and lift off of the whole NW-PDMS film. Fig. 5b shows the final result of dual-phase NW-PDMS WGPs patterned on a single PDMS sheet with a clearly defined boundary between the two sessions. The demonstration of polarizer performance shows that both top and bottom parts exhibit a clear contrast between TM and TE. This feature verifies the promise of this technique as a variety of substrates can be easily printed to have a polarizing effect.

Conclusions

In summary, we report a new simple and robust approach to make printable, mechanically deformable, and stretchable WGPs by integrating NW arrays with non-conventional organic/elastomer substrates using a multiple printing method assisted by sacrificial layers. By varying the geometrical parameters of the NW array, we provided a comprehensive understanding on the performance of bottom-up assembled WGPs designed from semiconductor NW arrays. Particularly, we found that the transmission spectrum of NW WGP can be altered by controlling the NW diameter distribution. The polarizer performance is examined under various deformations revealing high mechanical adaptability of NW-PDMS polarizers without any significant performance deterioration. Particularly, the significance of our new methodology and fabrication method is its potential in both diverse material choices and a scalable NW transfer method, like roll-to-roll processing. For instance, to further improve the performance of NW-PDMS polarizers, especially to enhance higher TM transmission and broader band characteristics, metallic shell coating on as-grown NWs (ESI: Fig. S5†) can be a promising method which is under investigation. We believe that the novelty in mechanical properties and the fabrication method adding to the potentially wide range of choices of one-dimensional materials and an expandable NW transfer scale can further extend our design platform to a broader range of applications and better performance in optical filters and sensors in wearable/mobile devices.

Acknowledgements

This research is supported by the Hellman Fellowship and Innovega Inc.

Notes and references

1 E. H. Land, *J. Opt. Soc. Am.*, 1951, **41**, 957.
2 M. D. Robinson, G. Sharp and J. Chen, *Polarization engineering for LCD projection*, John Wiley & Sons, 2005, vol. 4.
3 J. Shah, in High performance Silicon Photonics technology for ubiquitous communications: Intrachip to Data Warehouses, *Optical Interconnects Conference*, 2012, IEEE, pp. 112–112.
4 A. E. Hollowell and L. J. Guo, *Adv. Opt. Mater.*, 2013, **1**, 343.
5 X. Li, T. Gu and B. Wei, *Nano Lett.*, 2012, **12**, 6366.
6 A. J. Baca, J.-H. Ahn, Y. Sun, M. A. Meitl, E. Menard, H.-S. Kim, W. M. Choi, D.-H. Kim, Y. Huang and J. A. Rogers, *Angew. Chem., Int. Ed.*, 2008, **47**, 5524.
7 R. Agarwal, *Small*, 2008, **4**, 1872.
8 K. Yin, H. Lin, Q. Cai, Y. Zhao, S.-T. Lee, F. Hu and M. Shao, *Nanoscale*, 2013, **5**, 12330.
9 J.-H. Kim, Z. C. Y. Chen, S. Kwon and J. Xiang, *Nano Lett.*, 2014, **14**, 1687.
10 M. C. Wingert, Z. C. Y. Chen, E. Dechaumphai, J. Moon, J.-H. Kim, J. Xiang and R. Chen, *Nano Lett.*, 2011, **11**, 5507.
11 S.-K. Kim, R. W. Day, J. F. Cahoon, T. J. Kempa, K.-D. Song, H.-G. Park and C. M. Lieber, *Nano Lett.*, 2012, **12**, 4971.
12 G. Zheng, F. Patolsky, Y. Cui, W. U. Wang and C. M. Lieber, *Nat. Biotechnol.*, 2005, **23**, 1294.
13 D. Whang, S. Jin, Y. Wu and C. M. Lieber, *Nano Lett.*, 2003, **3**, 1255.
14 Y. Huang, X. Duan, Q. Wei and C. M. Lieber, *Science*, 2001, **291**, 630.
15 D. Zopes, R. von Hagen, R. Muller, R. Fiz and S. Mathur, *Nanoscale*, 2010, **2**, 2091.
16 S. Batra and M. Cakmak, *Nanoscale*, 2015, **7**, 20571.
17 R. K. Joshi and J. J. Schneider, *Chem. Soc. Rev.*, 2012, **41**, 5285.
18 A. Javey, R. S. Nam, H. Y. Friedman and C. M. Lieber, *Nano Lett.*, 2007, **7**, 773.
19 A. Nadarajah, R. C. Word, J. Meiss and R. Konenkamp, *Nano Lett.*, 2008, **8**, 534.
20 B. P. Timko, T. Cohen-Karni, G. Yu, Q. Qing, B. Tian and C. M. Lieber, *Nano Lett.*, 2009, **9**, 914.
21 X. Lu, G. Wang, T. Zhai, M. Yu, S. Xie, Y. Ling, C. Liang, Y. Tong and Y. Li, *Nano Lett.*, 2012, **12**, 5376.
22 G. Brönstrup, N. Jahr, C. Leiterer, A. Csáki, W. Fritzsche and S. Christiansen, *ACS Nano*, 2010, **4**, 7113.
23 C. J. Barrelet, A. B. Greytak and C. M. Lieber, *Nano Lett.*, 2004, **4**, 1981.
24 L. Cao, J. S. White, J. S. Park, J. A. Schuller, B. M. Clemens and M. L. Brongersma, *Nat. Mater.*, 2009, **8**, 643.
25 F. Qian, Y. Li, S. Gradečak, H.-G. Park, Y. Dong, Y. Ding, Z. L. Wang and C. M. Lieber, *Nat. Mater.*, 2008, **7**, 701.

26 K. Seo, M. Wober, P. Steinvurzel, E. Schonbrun, Y. Dan, T. Ellenbogen and K. B. Crozier, *Nano Lett.*, 2011, **11**, 1851.
27 L. Zhang, X. Dou, C. Min, Y. Zhang, L. Du, Z. Xie, J. Shen, Y. Zeng and X. Yuan, *Nanoscale*, 2016, **8**, 9756.
28 Y. Yu, V. Protasenko, D. Jena, H. Xing and M. Kuno, *Nano Lett.*, 2008, **8**, 1352.
29 A. Singh, X. Li, V. Protasenko, G. Galantai, M. Kuno, H. Xing and D. Jena, *Nano Lett.*, 2007, **7**, 2999.
30 H. E. Ruda and A. Shik, *Phys. Rev. B: Condens. Matter*, 2005, **72**, 115308.
31 P. M. van Midwoud, A. Janse, M. T. Merema, G. M. Groothuis and E. Verpoorte, *Anal. Chem.*, 2012, **84**, 3938.
32 Z. Fan, J. C. Ho, Z. A. Jacobson, R. Yerushalmi, R. L. Alley, H. Razavi and A. Javey, *Nano Lett.*, 2008, **8**, 20.
33 I. Abdulhalim, *Small*, 2014, **10**, 3499.
34 Y. Lin, X. Zhang, X. Fang and S. Liang, *Nanoscale*, 2016, **8**, 1421.
35 K. Lee and Q.-H. Park, *Phys. Rev. Lett.*, 2005, **95**, 103902.
36 J. Fréchette and C. Carraro, *Phys. Rev. B: Condens. Matter*, 2006, **74**, 161404.
37 L. Cao, P. Fan, A. P. Vasudev, J. S. White, Z. Yu, W. Cai, J. A. Schuller, S. Fan and M. L. Brongersma, *Nano Lett.*, 2010, **10**, 439.
38 C. A. Schneider, W. S. Rasband and K. W. Eliceiri, *Nat. Methods*, 2012, **9**, 671.
39 C. Ayres, G. L. Bowlin, S. C. Henderson, L. Taylor, J. Shultz, J. Alexander, T. A. Telemeco and D. G. Simpson, *Biomaterials*, 2006, **27**, 5524.
40 H. R. Philipp and E. A. Taft, *Phys. Rev.*, 1959, **113**, 1002.
41 L. T. Ngo, D. Almécija, J. E. Sader, B. Daly, N. Petkov, J. D. Holmes, D. Erts and J. J. Boland, *Nano Lett.*, 2006, **6**, 2964.
42 D. A. Smith, V. C. Holmberg and B. A. Korgel, *ACS Nano*, 2010, **4**, 2356.